PHYSICAL REVIEW B **81**, 195434 (2010)

# Quantum oscillations and quantum Hall effect in epitaxial graphene

Johannes Jobst,[1] Daniel Waldmann,[1] Florian Speck,[2] Roland Hirner,[2] Duncan K. Maude,[3] Thomas Seyller,[2] and Heiko B. Weber[1,*]

[1]*Lehrstuhl für Angewandte Physik, Universität Erlangen-Nürnberg, 91056 Erlangen, Germany*

[2]*Lehrstuhl für Technische Physik, Universität Erlangen-Nürnberg, 91056 Erlangen, Germany*

[3]*Laboratoire des Champs Magnétiques Intenses, 25 Avenue des Martyrs, 38042 Grenoble, France*

(Received 13 August 2009; revised manuscript received 12 March 2010; published 25 May 2010)

We investigate the transport properties of high-quality single-layer graphene, epitaxially grown on a 6H-SiC(0001) substrate. We have measured transport properties, in particular charge-carrier density, mobility, conductivity, and magnetoconductance of large samples as well as submicrometer-sized Hall bars which are entirely lying on atomically flat substrate terraces. The results display high mobilities, independent of sample size. The temperature dependence of the conductance indicates a rather strong coupling to the SiC substrate. An analysis of the Shubnikov-de Haas effect yields the Landau-level spectrum of single-layer graphene. When gated close to the Dirac point, the mobility increases substantially and the graphenelike quantum Hall effect occurs.

DOI: 10.1103/PhysRevB.81.195434 PACS number(s): 73.43.−f, 72.20.My

## I. INTRODUCTION

Graphene, a single sheet of graphite, is one of the most exciting electronic materials in the last years.[1] The observation of very fast charge carriers even at room temperature and unconventional quantum mechanics have stimulated far reaching visions in science and technology. Many of these properties are a direct consequence of the unique symmetry of graphene and its true two dimensionality. A calculation of the single-particle band structure delivers a linear $E(k)$ dispersion relation and a chiral degree of freedom in the electronic wave function. This *graphene physics* modifies, for example, the quantum Hall effect (QHE) (Refs. 2 and 3) and efficiently suppresses backscattering of charge carriers.[4–6]

There are today two main preparation strategies for graphene, resulting in different materials. *Mechanical exfoliation* of single graphene sheets from graphite yields small flakes a few tens of microns in size which are usually deposited on a silicon wafer covered by a layer of silicon oxide allowing for electrostatic gating. Since its discovery in 2004, *exfoliated graphene* has been the driving force for the exploration of graphene physics. Remarkably, a broad agreement between experiment and theory has been observed.

The second strategy is *epitaxial growth* of graphene on well defined surfaces. This procedure promises large-scale fabrication, detailed surface-science control, and would offer technological perspectives. Epitaxial graphene is currently developed into two major directions. Chemical vapor deposition on Ni, for instance, has been demonstrated to lead to graphene flakes which could be transferred to an insulating substrate. In this case, QHE typical for graphene was observed.[7] Another method uses the temperature-induced decomposition of the wide band-gap semiconductor silicon carbide (SiC).[8–10] Since SiC can be obtained in an insulating state, this technique does not require transferring the graphene layer onto another substrate, which is a clear technological advantage.

Epitaxial growth on SiC has been carried out on both polar surface orientations. Not unexpected, the growth and the resulting layers are dissimilar in many aspects. On the carbon terminated surface (C-face) the decomposition is rapid and often multilayers are grown. Transport studies of multilayered epitaxial graphene (MLEG) on the C-face of SiC have shown SdH oscillations of graphene monolayers and high electron mobility, but no QHE,[9] which is a consequence of the mutual rotation of the graphene layers within the stack.[11,12] On the silicon-terminated face (Si-face), growth of graphene is slower allowing for a controlled single-layer growth. The better thickness control achieved on Si-face SiC substrates yielding single layers is of particular importance for top-gated field effect devices as compared to thick stacks of MLEG (Ref. 13) due to screening.

As a consequence, we have concentrated on the growth of single-layer graphene on Si-face SiC. We studied extensively its surface with angle resolved photoemission (ARPES), scanning tunneling microscopy, low-energy electron diffraction, Raman spectroscopy, and first transport experiments.[10] Altogether a picture has been developed that this material has excellent quality and fits well to the graphene-model band structure. An anomaly in the ARPES spectra of epitaxial graphene on SiC(0001) has been interpreted as the signature of many-particle interactions.[14] However, a different interpretation of ARPES (Ref. 15) results suggest a symmetry breaking between A and B sublattices of graphene and subsequent formation of a band gap induced by the presence of the so-called buffer layer or $(6\sqrt{3}\times 6\sqrt{3})R30°$ reconstruction. If this were true, the nature of electrons in epitaxial graphene would be different from free graphene. The buffer layer forms the intrinsic interface between SiC(0001) and thermally grown graphene. The interface layer is semiconducting, i.e., has no states at the Fermi level, and we have proposed that it consists of a covalently bound graphene layer.[16] The higher-order commensurate unit cell (supercell) of the combined system graphene on buffer layer on SiC(0001) contains $13\times 13$ unit cells of graphene. It remains an unresolved question, whether this lowered symmetry spoils the graphene physics, for example by inducing a band gap.

To discover the graphene physics in our system, we carried out classical Hall effect, Shubnikov-de Haas (SdH) ef-

 

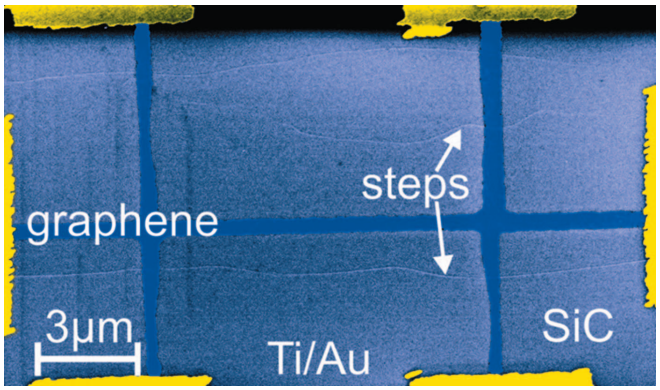


FIG. 1. (Color) Scanning electron micrograph of a Hall bar (0.48 $\mu$m width) lithographically patterned out of a single layer of graphene (dark blue) on an atomically flat substrate terrace of semi-insulating SiC. The substrate steps are clearly resolved.

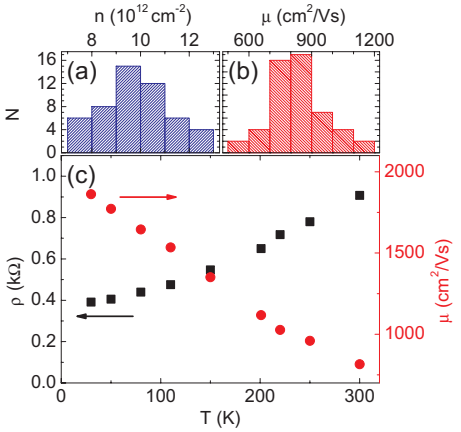


FIG. 2. (Color) (a) and (b) Histograms of charge-carrier density $n$ and charge-carrier mobility $\mu$ in epitaxial graphene for 51 samples of various sizes at room temperature. Both quantities have been determined by Hall effect measurements. (c) Temperature dependence of resistivity $\rho$ and mobility $\mu$ of a typical Hall bar sample. The resistivity increases superlinearly with increasing $T$, while $\mu$ decreases linearly.

fect and QHE measurements. The latter phenomena give a fingerprint of single-layer graphene behavior,[17] clearly different from parabolic band structures or nonchiral wave functions. We investigated the raw material as well as epitaxial graphene driven close to charge neutrality by chemical gating.

## II. TRANSPORT MEASUREMENTS AT THE PRISTINE MATERIAL

The growth process and the patterning has been reported in Ref. 10. Briefly, we have produced graphene on the silicon-terminated side of semi-insulating SiC by thermal decomposition at 1650 °C and 900 mbar argon atmosphere for ≈15 min. Then we have removed the graphene partly by electron beam lithography and subsequent oxygen plasma etching such that Hall bars of different sizes were patterned. Figure 1 shows a scanning electron micrograph of a sample with the Hall bar entirely placed on a single, atomically flat substrate terrace of the SiC(0001) surface. Here, we obtain reliably single-sheet graphene, as we keep some distance from the step edges.[10] Other samples were much larger, included many substrate steps and some even visible defects.

The electrical contacts were guided away from the Hall bar by graphene leads, and further out with metallic top contacts (Ti/Au). The samples were investigated in a cryostat fitted with a 0.66 T magnet, or in the high-field laboratory in Grenoble in magnetic fields up to 28 T.

The quantities which can be derived from Hall bar measurements are charge-carrier densities and charge-carrier mobilities. Figures 2(a) and 2(b) shows data derived for 51 samples of different sizes with the raw material. The charge-carrier density of $n \approx 10^{13}$ cm$^{-2}$ and a mobility at room temperature of $\mu \approx 900$ cm$^2$/Vs is found for all samples. The charge-carrier density can be related to electronlike transport with a chemical potential ≈380 meV above the Dirac point. This value is slightly below the photoemission result of ≈450 meV.[10] Surprisingly, the mobility of rather large samples and of Hall bars placed on a single substrate step does not differ noticeably. Although it is known that graphene grows over step edges without being disrupted,[9,18] it is surprising that the inhomogeneity does not affect global transport properties significantly.

Graphene is a very surface sensitive material. Hence, one may believe that the limitation of mobility might be caused by surface adsorbates. We heated up four samples to 350 °C for 30 min in cryogenic vacuum, in order to desorb potential adsorbates and continued the measurement without breaking the cryogenic vacuum. The measured quantities $n$ and $\mu$ remained essentially unaltered. Hence, adsorbates do not play a major role in our experiments Fig. 2(c). Further insight is gained from the temperature dependence of resistivity. It shows a superlinear behavior as reported for exfoliated graphene,[19] but the temperature-dependent contribution $\Delta\rho = \rho(300\ \mathrm{K}) - \rho(0\ \mathrm{K}) \approx 500\ \Omega$ is one order of magnitude larger. Hence, even if the residual resistivity $\rho(0\ \mathrm{K})$ could be eliminated by improved sample preparation, the temperature-dependent scattering mechanism would limit the room-temperature mobility to $\mu(300\ \mathrm{K}) \approx 1\,600$ cm$^2$/Vs. $\rho(0\ \mathrm{K})$ presumably stems from imperfections, and may be related to atomically sharp defects (a nonvanishing amplitude of the $D$ peak has also been observed in Raman spectroscopy)[10] while we attribute $\Delta\rho$ to interactions with substrate phonons. Note also that the mobility plotted against $T$ is remarkably linear.

In a further experiment, we measured the magnetoresistance in higher magnetic fields up to 28 T at cryogenic temperatures ($1.4\ \mathrm{K} < T < 4.2\ \mathrm{K}$). In this regime, electronic degrees of freedom are condensed in Landau levels, which in graphene have a significantly different spectrum compared to other materials.[17] Figure 3(a) shows the magnetoresistance $R_{xx}$ and the Hall resistance $R_{xy}$ as a function of magnetic field $B$. With increasing field, the evolution of $R_{xx}$ to quantum oscillations can clearly be seen. The quantum Hall regime, however, with $R_{xx}=0$ is not yet reached in this sample with a charge density $n = 8.9 \times 10^{12}$ cm$^{-2}$ and $\mu = 2\,300$ cm$^2$/Vs. $R_{xy}$ already displays plateaus, which are precursors of the quantum Hall effect.

The values of these plateaus fit in the scheme of $R_{xy} = h/(4n+2)e^2$ with $n$ being the Landau-level index, as found

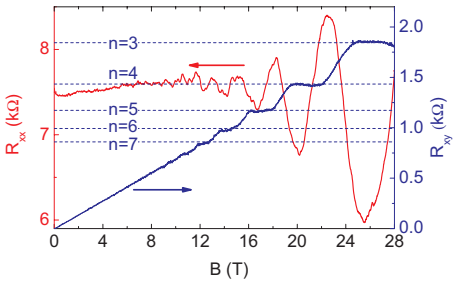


FIG. 3. (Color) Resistance $R_{xx}$ and Hall resistance $R_{xy}$ at $T=4.2$ K from a sample of single-sheet graphene, entirely placed on a single substrate step (Fig. 1). $R_{xx}$ shows Shubnikov-de Haas oscillations, but no quantum Hall effect. The Hall resistance, however, shows steplike plateaus such as in the quantum Hall effect. Plateau values and the positions of extrema can be identified with the unconventional Landau-level structure of single-layer graphene.

in exfoliated graphene. When the positions of the associated maxima (minima) in $R_{xx}$ are plotted against the inverse field $1/B$ [Fig. 4 (circles)], a linear dependence can be recognized. The axis intercept is $\beta=n(B\rightarrow\infty)=1/2$ ($\beta=0$), as expected and experimentally confirmed for electrons in exfoliated graphene (often, this is described as the geometric Berry phase $\pi$ associated to a closed orbit). Hence, the SdH oscillations in the raw material (380 meV above the charge neutrality point) display graphene physics. Note that the expectations of the Berry phase in bilayer graphene would be $2\pi$.

## III. MEASUREMENTS CLOSE TO THE DIRAC POINT: HIGH MOBILITIES

The most interesting part of the graphene spectrum is the Dirac point, or the charge neutrality point, where the density of state shrinks to zero, and the charge-carrier mobility may become huge.[3] As we have currently no tunable gate available, we used a static gate by depositing thermally evaporated tetrafluoro-tetracyanoquinodimethane (F4-TCNQ) molecules. Upon contact these acceptor-molecules are reduced and effectively drive the graphene close to the charge neutrality point.[20] We have chosen a thickness close to a monolayer (see below), for which the sample is reasonable stable. However, some drift in $n$ occurs within days, accompanied by increasing inhomogeneities. Classical Hall effect measurements of the sample with the lowest $n=5.4\times10^{10}$ cm$^{-2}$ displayed excellent mobilities of $\mu=29\,000$ cm$^2$/Vs at $T=25$ K, as shown in Fig. 5 (closed symbols). Note that for rising temperatures, not only electrons, but also hole states are accessible by the Fermi distribution. As a consequence, the evaluation of the Hall data has to consider two charge-carrier types, so $\mu$ and $n$ cannot be unambiguously derived. When assuming a two-band model ($\mu_{holes}=\mu_{electrons}$ for simplicity), the resulting simulation describes the temperature dependence reasonably well (star symbols in Fig. 5). The expectation would be that even higher mobilities are achievable, if one would come closer to the Dirac point. Mobilities over 20 000 cm$^2$/Vs are rarely found for exfoliated graphene on a substrate and significantly better values are only found in absence of a substrate.[21] Here, high mobilities are observed although the graphene is in contact with two surfaces: the SiC substrate with its large supercell and the virtually disordered F4-TCNQ film on top.

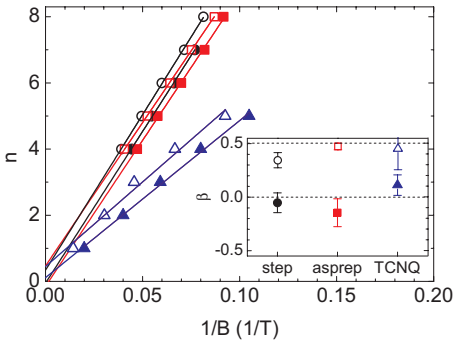


FIG. 4. (Color) Landau-level index $n$ of the SdH maxima (closed symbols) and minima (open symbols) over the inverse magnetic field $1/B$ and linear fits. Circles: as-prepared sample lying on a single substrate terrace. Squares: as-prepared sample covering several substrate steps. Triangles: sample gated close to charge neutrality with F4-TCNQ (plotted against $0.1/B$ for clarity). Inset: the axis intercepts of $\beta=0.5$ and $\beta=0$ for minima and maxima, respectively, yield a Berry phase of $\pi$ as expected for single-layer graphene. The error bars indicate the standard deviation of the fitting constant.

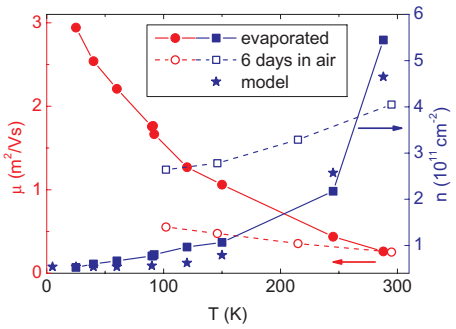


FIG. 5. (Color) Charge-carrier mobility $\mu$ and density $n$ for a sample close to the charge neutrality point ($E_F=27$ meV). Closed symbols: $\mu$ (red) and $n$ (blue) derived from an evaluation of Hall data, assuming only one charge-carrier type, yields mobilities of 29 000 cm$^2$/Vs. The strong temperature dependence comes from the interplay of electrons and holes in the Fermi distribution at finite temperatures. A simple two-band model (open squares) yields a similar $T$ dependence. Open symbols: the same sample after exposure to air for six days ($E_F=59$ meV) (open squares). We attribute the higher $n$ and reduced $\mu$ to the degradation of the F4-TCNQ layer.

For a detailed understanding of the underlying material, we have carried out extensive studies of the F4-TCNQ layer and its action on the graphene layer by photoemission spectroscopy. Here, we will focus on x-ray photoemission spectroscopy (XPS) measurements of the highest-mobility sample. The data were taken on a designated area of the SiC chip not far from the Hall bar. It was thus treated by the same lithography processes, but unpatterned. First, graphene was grown on the entire chip by the Ar growth process described in.[10] Then PMMA was spin coated all over the chip. Two lithography steps, including an oxygen etch and the addition

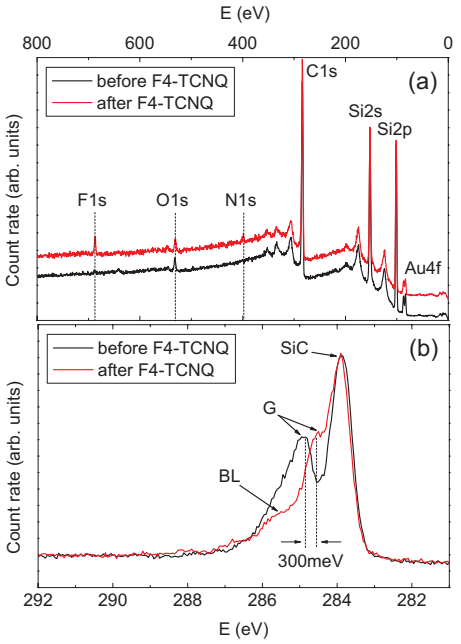


FIG. 6. (Color) XPS spectra of a sample before and after application of F4-TCNQ molecules. In the survey spectrum (a) additional F 1*s* an N 1*s* peaks are found after evaporation of F4-TCNQ (spectra shifted for clarity). A closer look to the C 1*s* peak (b) shows signals of the SiC substrate (SiC) and the BL. The shift of the graphene peak (g) due to the F4-TCNQ doping is clearly visible.

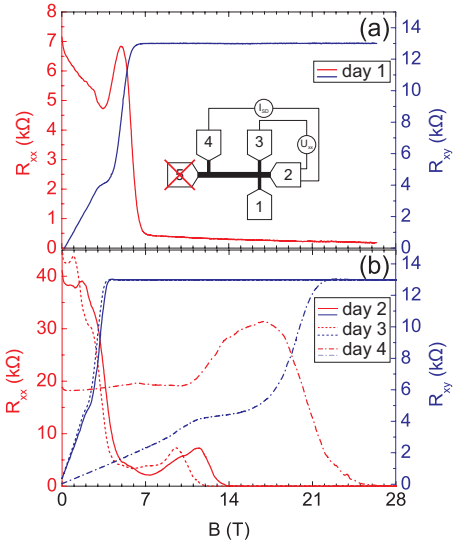


FIG. 7. (Color) Resistance $R_{xx}$ and Hall resistance $R_{xy}$ at $T=4.2$ K in a sample doped close to charge neutrality by F4-TCNQ. (a) Shubnikov-de Haas oscillations (barely visible below 4 T) and quantum Hall effect are present and demonstrate the unique single-layer graphene properties. Due to a lost wire $R_{xx}$ was measured on day 1 in a three-terminal geometry (see inset). Contact and wiring give rise to an additional resistance of $\approx 300\ \Omega$. $R_{xy}$, however, is measured correctly. (b) The same sample with repaired contact wire measured during the following days. Day 2 (solid line) and day 3 (dashed line) show that for high $B$ $R_{xx}$ becomes essentially zero. Additional peaks arise in $R_{xx}$, probably due to increasing inhomogeneities. Day 4 (dashed-dotted line) shows data after rinsing the sample in water. The inhomogeneities become more pronounced but QHE effect is still visible for $B > 26$ T.

of metallic contact pads were carried out. Then the remaining PMMA was removed by rinsing in acetone/isopropanol. At this stage, the first XPS data were taken. Then, F4-TCNQ was thermally evaporated on the whole chip area in a vacuum chamber (base pressure $\approx 10^{-7}$ mbar). Again, XPS data were taken on the unpatterned part of the chip and electrical measurements were undertaken at the Hall bar.

Figure 6(a) shows XPS data before and after the application of F4-TCNQ molecules. Before, the C 1*s*, Si 2*s*, and Si 2*p* peaks of the underlying substrate are clearly visible. In contrast to as-grown graphene oxygen is detectable as well. We attribute this to the incomplete removal of PMMA. Also, some gold is detected, which stems from the electrical leads being partially detected. After the application of molecules, F 1*s* and N 1*s* core levels can also be seen, indicating the presence of F4-TCNQ molecules. From the attenuation of the Si 2*p* core level we estimate the thickness of the F4-TCNQ layer to be $0.5 \pm 0.2$ nm, i.e., in the monolayer regime for this particular sample. Figure 6(b) displays the C 1*s* core level spectrum before and after deposition of F4-TCNQ. The spectrum taken before F4-TCNQ deposition shows the typical shape of monolayer graphene grown on SiC(0001).[16] The spectrum is made up from components due to the SiC substrate (SiC), the graphene layer (G), and the buffer layer (BL). Details are discussed in Ref. 16. The graphene peak is located at a binding energy of 284.85 eV due to *n*-type doping.[16] After the evaporation, the graphene peak is clearly shifted by $0.3 \pm 0.05$ eV toward lower binding energy. This indicates a shift of the Fermi level toward the Dirac point due to the removal of excess charge by transfer to the F4-TCNQ molecules.[20] The binding energy of the graphene C 1*s* signal of 284.55 eV corresponds to a carrier density of $\approx 7 \times 10^{11}$ cm$^{-2}$, which fits well to the charge density derived from the Hall measurements. From the XPS data we can, however, not decide how homogeneous the coverage is. The PMMA residues may cause inhomogeneities in the charge density of the graphene layer: the graphene areas being immediately in contact with F4-TCNQ are driven close to the charge neutrality point whereas the small areas being contaminated by PMMA residues presumably have higher electronlike charge densities.

Figure 5 (open symbols) shows the temperature dependence of charge density $n$ and mobility $\mu$ of the high-mobility sample described above. After the first measurement the sample was exposed to air for six days. Afterwards a slightly higher charge-carrier density $n$ was measured. We attribute this to a degradation of the F4-TCNQ coverage and therefore a reduction in the doping, presumably accompanied by increasing inhomogeneities. The charge density depends also less on temperature than in the first measurement. This is not unexpected as for higher $E_F$ the influence of thermally activated charge carriers is reduced. When shifting away from charge neutrality the mobility $\mu$ is considerably smaller, but still higher than for undecorated (without F4-TCNQ) graphene samples.

## IV. MEASUREMENTS CLOSE TO THE DIRAC POINT: MAGNETOOSCILLATIONS AND QUANTUM HALL EFFECT

We further pursued measurements in high magnetic field with a F4-TCNQ covered sample. These data were collected in Grenoble, the sample preparation was carried out in Erlangen. To cope with the effect of degradation, we started the measurements in Grenoble with a new F4-TCNQ covered graphene sample, ≈30 h after preparation. The sample was originally fitted with five wires to carry out conductance and Hall measurements in four-terminal geometry. Unfortunately, the sample under investigation lost one bond wire during contacting and cooldown. The measurement was then carried out such that the source in the Hall bar was replaced by lead 4 [see sketch in Fig. 7(a)]. Hence, the Hall resistance $R_{xy}$ was measured correctly, but the longitudinal resistance $R_{xx}$ was effectively measured in a three-terminal measurement. Consequently, the wire resistance plus the contact resistance occur in the measurement of $R_{xx}$.

Figure 7(a) shows the magnetoresistance $R_{xx}$ and the Hall resistance $R_{xy}$ of this F4-TCNQ covered sample. It was slightly filled with electrons ($n=4.9\times10^{11}$ cm$^{-2}$, $\mu=4\,900$ cm$^2$/Vs at $T=4.2$ K). In the low-field regime, Shubnikov-de Haas oscillations occur. Compared to Fig. 3, the quantum oscillations are rather compressed as a consequence of the low charge-carrier density. For magnetic fields larger than 7 T, the resistance has small value of 300 Ω at high magnetic fields, which gives essentially $R_{xx}\approx0$, taken the experimental imperfection into account. In these fields, the Hall resistance has a value very close to $h/2e^2$. This can be identified as the last plateau of the QHE. From this single plateau, it can be derived that the QHE is different from bilayer graphene, where it should be $h/4e^2$. Further information about the Landau-level spectrum can be gained by analyzing the SdH oscillations similar to the above procedure: a SdH phase is found which corresponds to a Berry phase of $\pi$ (Fig. 4). This is a central result of our investigations: the quantum Hall effect has been observed in epitaxial graphene. It displays the same unique features as in model graphene, even close to the Dirac point, which is most sensitive to symmetry perturbations. It should be emphasized these data explicitly exclude a relevant symmetry breaking with a gap of 0.26 eV, as suspected from ARPES data.[15]

The following day we managed to repair the lost bond wire and repeated the measurement, this time in a standard five wire configuration. These data are displayed in Fig. 7(b) (solid red line). It is confirmed that $R_{xx}$ becomes essentially zero for high magnetic fields, as it is expected in the quantum Hall regime. However, this data set displays an unexpected feature between 7 and 14 T and more importantly, the SdH oscillations are blurred. We attribute this to the increased inhomogeneity associated to the warmup and cooldown, and the elapsed time. On day 3, the measurement was repeated, resulting again in modified $R_{xx}$ data, which underscores our interpretation. We have the impression that water plays an important role in the degradation process. To illustrate this, we finally rinsed the sample in water (resulting in a partial removal of F4-TCNQ), and measured again the magnetoconductance [dashed-dotted lines in Fig. 7(b)]. The Shubnikov-de Haas oscillations are fully destroyed and all features shift considerably to higher magnetic fields. Interestingly even for this obviously inhomogeneous sample, the quantum Hall effect still survives above 26 T.

It is remarkable that all samples show quantum oscillations typical for single-layer graphene, although the F4-TCNQ covered Hall bar as well as one as-prepared sample did not lie on a single substrate terrace. Therefore parts of the sample are bilayers, which extend as small stripes along the step edges. Why the Landau-level structure is insensitive to these stripes is unclear.

## V. CONCLUSIONS

We conclude that the raw graphene material, which is strongly electron filled has a charge-carrier mobility around 900 cm$^2$/Vs at room temperature and 2 000 cm$^2$/Vs at low temperatures. This limitation comes partly from electron-phonon interaction with substrate phonons, partly from crystal imperfections. The mobility is insensitive to substrate steps. Shubnikov-de Haas oscillations and plateaus in the Hall resistance indicate that at $B=28$ T the quantum Hall regime is not yet fully reached, but the Landau-level spectrum is (single-sheet) graphenelike.

When gating close to the Dirac point, high mobilities of 29 000 cm$^2$/Vs are observed. The quantum oscillations in high magnetic fields reveal the Landau-level spectrum of single-sheet graphene, and the graphenelike quantum Hall effect is observed. Hence, epitaxial graphene reproduces the unique features observed in exfoliated graphene even very close to charge neutrality point, but is certainly a system which allows for more systematic development of graphene devices, with rich perspectives for science and technology.

## ACKNOWLEDGMENTS

We gratefully acknowledge support by the DFG under contract No. SE 1087/5-1, WE 4542-5-1, and within the Cluster of Excellence *Engineering of Advanced Materials* (www.eam.uni-erlangen.de). This work has been partially supported through EUROMAGNET II under SP7 of the EU under contract number 228043. During the review process of this manuscript, two publications appeared displaying quantum Hall effect in epitaxial graphene on SiC, both at intermediate charge density, hence considerably more distant from charge neutrality.[22,23] In particular, Ref. 22 measured the quantum Hall resistance with very high accuracy.

*heiko.weber@physik.uni-erlangen.de

[1] A. K. Geim and K. S. Novoselov, Nature Mater. **6**, 183 (2007).
[2] K. S. Novoselov, A. K. Geim, S. V. Morozov, D. Jiang, M. I. Katsnelson, I. V. Grigorieva, S. V. Dubonos, and A. A. Firsov, Nature (London) **438**, 197 (2005).
[3] Y. Zhang, Y.-W. Tan, H. L. Stormer, and P. Kim, Nature (London) **438**, 201 (2005).
[4] T. Ando and T. Nakanishi, J. Phys. Soc. Jpn. **67**, 1704 (1998).
[5] M. I. Katsnelson, K. S. Novoselov, and A. K. Geim, Nat. Phys. **2**, 620 (2006).
[6] A. F. Young and P. Kim, Nat. Phys. **5**, 222 (2009).
[7] K. S. Kim, Y. Zhao, H. Jang, S. Y. Lee, J. M. Kim, K. S. Kim, J.-H. Ahn, P. Kim, J.-Y. Choi, and B. H. Hong, Nature (London) **457**, 706 (2009).
[8] I. Forbeaux, J.-M. Themlin, and J.-M. Debever, Phys. Rev. B **58**, 16396 (1998).
[9] C. Berger *et al.*, Science **312**, 1191 (2006).
[10] K. V. Emtsev *et al.*, Nature Mater. **8**, 203 (2009).
[11] J. Hass, F. Varchon, J. E. Millan-Otoya, M. Sprinkle, N. Sharma, W. A. de Heer, C. Berger, P. N. First, L. Magaud, and E. H. Conrad, Phys. Rev. Lett. **100**, 125504 (2008).
[12] S. Shallcross, S. Sharma, and O. A. Pankratov, Phys. Rev. Lett. **101**, 056803 (2008).
[13] J. Kedzierski, P.-L. Hsu, P. Healey, P. W. Wyatt, C. L. Keast, M. Sprinkle, C. Berger, and W. A. de Heer, IEEE Trans. Electron Devices **55**, 2078 (2008).
[14] A. Bostwick, T. Ohta, T. Seyller, K. Horn, and E. Rotenberg, Nat. Phys. **3**, 36 (2007).
[15] S. Y. Zhou, G.-H. Gweon, A. V. Fedorov, P. N. First, W. A. de Heer, D.-H. Lee, F. Guinea, A. H. C. Neto, and A. Lanzara, Nature Mater. **6**, 770 (2007).
[16] K. V. Emtsev, F. Speck, T. Seyller, L. Ley, and J. D. Riley, Phys. Rev. B **77**, 155303 (2008).
[17] K. S. Novoselov, E. McCann, S. V. Morozov, V. I. Fal'ko, M. I. Katsnelson, U. Zeitler, D. Jiang, F. Schedin, and A. K. Geim, Nat. Phys. **2**, 177 (2006).
[18] P. Lauffer, K. V. Emtsev, R. Graupner, T. Seyller, L. Ley, S. A. Reshanov, and H. B. Weber, Phys. Rev. B **77**, 155426 (2008).
[19] S. V. Morozov, K. S. Novoselov, M. I. Katsnelson, F. Schedin, D. C. Elias, J. A. Jaszczak, and A. K. Geim, Phys. Rev. Lett. **100**, 016602 (2008).
[20] W. Chen, S. Chen, D. C. Qi, X. Y. Gao, and A. T. S. Wee, J. Am. Chem. Soc. **129**, 10418 (2007).
[21] K. I. Bolotin, K. J. Sikes, J. Hone, H. L. Stormer, and P. Kim, Phys. Rev. Lett. **101**, 096802 (2008).
[22] A. Tzalenchuk, S. Lara-Avila, A. Kalaboukhov, S. Paolillo, M. Syväjärvi, R. Yakimova, O. Kazakova, T. J. B. M. Janssen, V. Fal'ko, and S. Kubatkin, Nat. Nanotechnol. **5**, 186 (2010).
[23] T. Shen, J. J. Gu, M. Xu, Y. Q. Wu, M. L. Bolen, M. A. Capano, L. W. Engel, and P. D. Ye, Appl. Phys. Lett. **95**, 172105 (2009).